

## ■ Porphyrinoids

Ytterbium(III) Porpholactones:  $\beta$ -Lactonization of Porphyrin Ligands Enhances Sensitization Efficiency of Lanthanide Near-Infrared LuminescenceXian-Sheng Ke,<sup>[a]</sup> Bo-Yan Yang,<sup>[a]</sup> Xin Cheng,<sup>[a]</sup> Sharon Lai-Fung Chan,<sup>[b]</sup> and Jun-Long Zhang\*<sup>[a]</sup>

**Abstract:** The near-infrared (NIR) luminescence efficiency of lanthanide complexes is largely dependent on the electronic and photophysical properties of antenna ligands. Although porphyrin ligands are efficient sensitizers of lanthanide NIR luminescence, non-pyrrolic porphyrin analogues, which have unusual symmetry and electronic states, have been much less studied. In this work, we used porpholactones, a class of  $\beta$ -pyrrolic-modified porphyrins, as ligands and investigated the photophysical properties of lanthanide porpholactones **Yb-1a–5a**. Compared with Yb porphyrin complexes, the porpholactone complexes displayed remarkable enhancement of NIR emission (50–120%). Estimating the triplet-state levels of porphyrin and porpholactone in Gd complexes revealed that  $\beta$ -lactonization of porphyrinic ligands lowers the ligand T<sub>1</sub> state and results in a narrow energy gap between this state and the lowest excited state of Yb<sup>3+</sup>. Transient ab-

sorption spectra showed that Yb<sup>III</sup> porpholactone has a longer transient decay lifetime at the Soret band than the porphyrin analogue (30.8 versus 17.0  $\mu$ s). Thus, the narrower energy gap and longer lifetime arising from  $\beta$ -lactonization are assumed to enhance NIR emission of Yb porpholactones. To demonstrate the potential applications of Yb porpholactone, a water-soluble Yb bioprobe was constructed by conjugating glucose to **Yb-1a**. Interestingly, the NIR emission of this Yb porpholactone could be specifically switched on in the presence of glucose oxidase and then switched off by addition of glucose. This is the first demonstration that non-pyrrolic porphyrin ligands enhance the sensitization efficiency of lanthanide luminescence and also display switchable NIR emission in the region of biological analytes (800–1400 nm).

## Introduction

Porphyrin analogues in which one pyrrolic subunit is replaced by a non-pyrrolic moiety have recently attracted much attention for their unusual electronic states and photophysical properties.<sup>[1]</sup> These replacements at the porphyrin periphery are strongly electronically coupled to the chromophores and thus make them attractive ligands. Despite the tremendous progress made in transition metal complexes of non-pyrrolic porphyrins,<sup>[1c,2]</sup> related studies on lanthanide (Ln) complexes have rarely been reported. It is well known that porphyrins are

promising antenna ligands for sensitizing near-infrared (NIR)-luminescent lanthanide complexes, because they absorb strongly both in the UV and visible regions.<sup>[3]</sup> However, the NIR emission efficiency has yet to be improved. Given that the energy levels of lanthanide ions are hardly affected by their environment, modulation of the electronic structures of porphyrinoids by replacing traditional pyrrolic moieties would be a viable way to tune NIR emission. To the best of our knowledge, the only examples thereof are the lanthanide complexes of N-confused porphyrin,<sup>[4]</sup> which display weaker NIR emission than their porphyrin congeners. This inspired us to explore the effect of pyrrolic replacement on lanthanide sensitization, and thus extend the chemistry of porphyrin derivatives containing non-pyrrolic moieties to lanthanides.

Porpholactones are a class of non-pyrrolic porphyrinoids in which a pyrrole moiety is replaced by an oxazolone group (or one porphyrin  $\beta,\beta'$ -double bond is replaced by a lactone moiety).<sup>[5]</sup> Their optical and photophysical properties are intermediate between those of porphyrin and chlorin<sup>[5b]</sup> when the oxa and oxo atoms are involved in the  $\pi$  conjugation of the system. This makes them suitable for optical application such as chemosensors for oxygen sensing in pressure-sensing materials,<sup>[6]</sup> pH indicators,<sup>[7]</sup> and reactive oxygen species.<sup>[8]</sup> Platinum(II) porpholactones show redshifted phosphorescence

[a] X.-S. Ke, B.-Y. Yang, X. Cheng, Prof. Dr. J.-L. Zhang  
Beijing National Laboratory for Molecular Sciences  
State Key Laboratory of Rare-Earth Materials Chemistry and Applications  
College of Chemistry and Molecular Engineering  
Peking University  
Beijing 100871 (P. R. China)  
Fax: (+86) 1062767034  
E-mail: zhangjunlong@pku.edu.cn

[b] Dr. S. L.-F. Chan  
Department of Applied Biology and Chemical Technology  
The Hong Kong Polytechnic University  
Hung Hom, Kowloon, Hong Kong (P. R. China)

Supporting information for this article is available on the WWW under <http://dx.doi.org/10.1002/chem.201303972>.

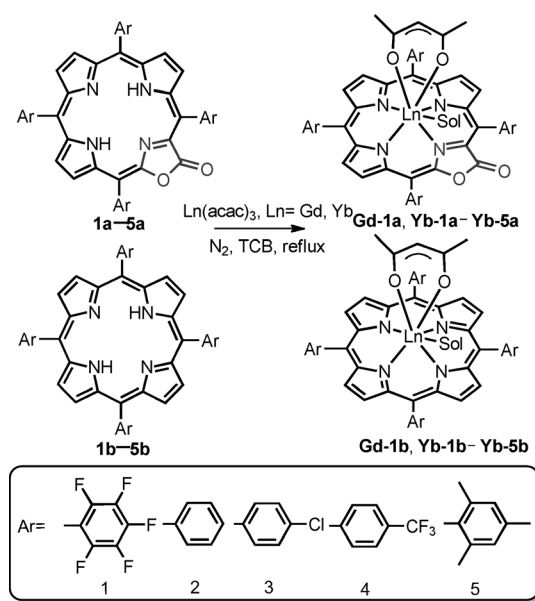
compared to porphyrin analogues, which indicates that  $\beta$ -lactonization of porphyrinic ligands affects the  $^3\text{MLCT}$  triplet excited state.<sup>[9]</sup>

Herein, we report the first synthesis of lanthanide porpholactone complexes. We found that  $\beta$ -lactonization of porphyrinic ligands leads to enhanced Yb NIR luminescence, longer lifetimes of Yb porpholactone complexes, and a smaller energy gap between the ligand  $T_1$  state (based on estimates of the levels of the ligand  $T_1$  states in Gd porphyrin and porpholactone) and the lowest excited states of  $\text{Yb}^{3+}$ .

To demonstrate potential applications, we were interested in the NIR emission window of 800–1400 nm, which has less interference from light scattering and autofluorescence of biological matter.<sup>[10]</sup> The  $\text{Yb}^{3+}$  ion was chosen because its electronic structure ( $f^{13}$  configuration) is relatively simple, the first excited state ( $^2F_{5/2}$ ) is located in the NIR region, and Yb porphyrins have higher quantum yields than Er and Nd analogues.<sup>[3c]</sup> In addition, Yb porphyrins exhibit higher stability than Er and Nd porphyrin analogues because of the smaller size of the  $\text{Yb}^{3+}$  ion (Shannon effective ionic radius: 0.985 Å). Recently, some water-soluble Yb porphyrin derivatives were found to display strong affinity towards DNA and to cleave DNA on photoactivation,<sup>[11]</sup> ytterbium porphyrin complexes conjugated with rhodamine B have been reported for imaging mitochondria,<sup>[12]</sup> and recently, Che and co-workers reported their potent anti-cancer activities with cytotoxic  $\text{IC}_{50}$  values down to the sub-micromolar range.<sup>[13]</sup> Despite the importance of the application of Yb porphyrinoids as NIR-emissive bioprobes for signaling and sensing the biological events in the NIR region, no example thereof has been reported in the literature. This is due to the fact that NIR emission from Yb porphyrins is well known to be quenched by small molecules with high-energy oscillators such as O–H bonds in water. We envisioned that, through appropriate molecular design, a certain analyte might protect  $\text{Ln}^{3+}$  cations against nonradiative deactivation induced by water and thus switch on the NIR emission. To demonstrate this, we prepared a water-soluble Yb porpholactone by conjugation with glucose and found the NIR emission was specifically switched on in the presence of glucose oxidase (GOx). Moreover, this switched-on emission could be quenched by the addition of glucose, and this suggests that the switched-on emission is due to selective binding of glucose conjugates to GOx.

## Results and Discussion

Ytterbium(III) complexes **Yb-1 a–5 a** (**1 a–5 a** = *meso*-tetrakis-(pentafluorophenyl)porpholactone, *meso*-tetraphenylporpholactone, *meso*-tetrakis(*p*-chlorophenyl) porpholactone, *meso*-tetrakis(*p*-trifluoromethylphenyl)porpholactone, and *meso*-tetramesitylporpholactone, respectively) and **Yb-1 b–5 b** (**1 b–5 b** = *meso*-tetrakis(pentafluorophenyl)porphyrin, *meso*-tetraphenylporphyrin, *meso*-tetrakis(*p*-chlorophenyl)porphyrin, *meso*-tetrakis(*p*-trifluoromethylphenyl)porphyrin, and *meso*-tetramesitylporphyrin, respectively) were synthesized according to the method of Wong<sup>[3a]</sup> with modifications (Scheme 1). In general, a mixture of  $\text{Ln}(\text{acac})_3$  and the corresponding free ligand was heated in 1,2,4-trichlorobenzene for 8 h to give an



**Scheme 1.** Representative porphyrins and porpholactones and synthetic route to Ln complexes. acac = acetylacetonate.

alytically pure lanthanide complexes after purification by column chromatography and recrystallization. Gadolinium complexes **Gd-1 a** and **Gd-1 b** were synthesized by a similar procedure.

The products were characterized by IR and UV/Vis spectroscopy and ESI mass spectrometry, and their purities were confirmed by elemental analysis. Data from ESI MS analysis in  $\text{CH}_2\text{Cl}_2/\text{CH}_3\text{OH}$  suggested a monomeric structure for all complexes with molecular formula of  $[\text{Ln}(\text{Por or Porp})(\text{acac})]$ . The FTIR spectra of **Yb-1 a–5 a** and **Gd-1 a** showed a C=O stretching band at 1778, 1759, 1772, 1769, 1761, and 1770  $\text{cm}^{-1}$ , respectively, indicating that the lactone moiety of porpholactone<sup>[5a]</sup> remains intact during metalation with the  $\text{Yb}^{3+}$  ion.

The photophysical properties of the Yb porpholactones were characterized by absorption and photoluminescence spectroscopy in dichloromethane (Table 1). Although Yb porphyrins were previously characterized, we measured their photophysical properties for comparison purposes. Figure 1a shows the absorption spectra of free bases **1 a** and **1 b**, **Yb-1 a**, and **Yb-1 b** in dichloromethane. Compared with the free bases, **Yb-1 a** and **Yb-1 b** displayed a moderate redshift (10 nm) of the Soret band and two moderately intense Q bands in the range of 550–700 nm, which are characteristic features of metalloporphyrins and metalloporpholactones. The major differences in absorption between **Yb-1 a** and **Yb-1 b** are a redshifted Q(0,0) band (15 nm) and the increased extinction coefficient (ca. 8-fold) for **Yb-1 a**. Figure 1b shows NIR emission spectra of **Yb-1 a** and **Yb-1 b** excited at 420 nm and the excitation spectra of **Yb-1 a** and **Yb-1 b** monitored at 972 nm in dichloromethane. Typical NIR emission centered at 972 nm arising from the  $^2F_{5/2} \rightarrow ^2F_{7/2}$  transition for  $\text{Yb}^{3+}$  was observed, along with weak fluorescence in the visible region (600–720 nm). At the same concentration ( $4 \times 10^{-6}$  M), **Yb-1 a** showed higher emission in-

Compound	Absorption $\lambda_{\text{max}}$ [nm] [lg( $\epsilon/\text{M}^{-1}\text{cm}^{-1}$ )]	Vis emission $\lambda_{\text{max}}$ [nm] ( $\tau$ [ns])	NIR emission $\lambda_{\text{max}}$ [nm]	$\Phi_{\text{tot}}$ [%] <sup>[b]</sup>	$\tau_{\text{obs}}$ [ $\mu\text{s}$ ] <sup>[c]</sup>	$\eta_{\text{Yb-a}}/\eta_{\text{Yb-b}}$ <sup>[d]</sup>
<b>Yb-1 a</b>	419 [5.51], 564 [4.09], 608 [4.63]	612 (3.21), 668 (3.45)	972, 1004, 1021	3.3	26.5	1.33
<b>Yb-1 b</b>	416 [5.62], 547 [4.29], 582 [3.71]	588 (2.95), 641 (3.22)	973, 1004, 1022	2.2	23.5	
<b>Yb-2 a</b>	425 [5.51], 561 [4.06], 606 [4.33]	609 (3.27), 667 (3.51)	973, 1006, 1022	2.8	27.0	1.59
<b>Yb-2 b</b>	422 [5.62], 552 [4.24], 589 [3.62]	607 (3.63), 650 (4.60)	974, 1002, 1023	1.6	24.5	
<b>Yb-3 a</b>	426 [5.55], 563 [4.12], 607 [4.46]	612 (2.59), 666 (3.67)	972, 1007, 1025	3.1	29.9	1.82
<b>Yb-3 b</b>	423 [5.62], 552 [4.27], 590 [3.71]	605 (2.63), 647 (4.45)	973, 1006, 1025	1.5	26.3	
<b>Yb-4 a</b>	424 [5.52], 563 [4.10], 607 [4.47]	615 (3.33), 670 (3.46)	972, 1007, 1024	4.1	25.5	1.70
<b>Yb-4 b</b>	421 [5.66], 553 [4.30], 592 [3.58]	611 (3.15), 648 (3.80)	973, 1006, 1025	2.5	26.5	
<b>Yb-5 a</b>	425 [5.53], 561 [4.14], 606 [4.56]	612 (4.02), 664 (4.02)	972, 1006, 1022	2.4	25.7	1.99
<b>Yb-5 b</b>	423 [5.67], 553 [4.33], 589 [3.47]	608 (3.88), 647 (4.35)	973, 1004, 1024	1.1	23.4	

[a] All the photophysical data were determined in anhydrous  $\text{CH}_2\text{Cl}_2$  at room temperature. [b] Quantum yields were measured by using YbTPP(Tp) as reference; the estimated error is  $\pm 15\%$ . [c] NIR luminescence lifetimes were monitored at 975 nm, and all decay curves were fitted to a double-exponential decay function. [d]  $\eta_{\text{Yb-a}}/\eta_{\text{Yb-b}}$  is the ratio of sensitization efficiencies of porpholactone **Yb-a** and porphyrin **Yb-b**.

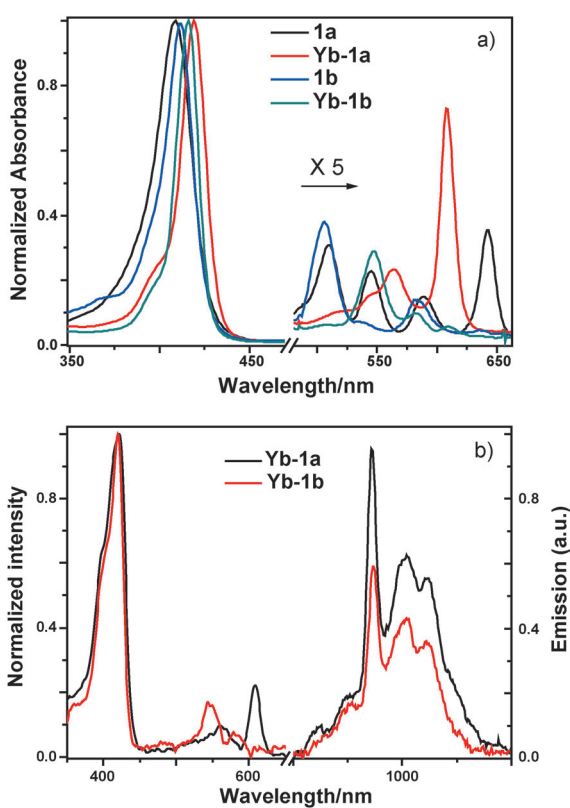


Figure 1. a) Normalized absorption of free bases **1 a**, **1 b** and Yb complexes **Yb-1 a** and **Yb-1 b** in  $\text{CH}_2\text{Cl}_2$ . b) NIR emission spectra of **Yb-1 a** and **Yb-1 b** ( $\lambda_{\text{ex}} = 420$  nm) at  $4 \times 10^{-6}$  M and excitation spectra monitored at 972 nm in  $\text{CH}_2\text{Cl}_2$ .

tensity than **Yb-1 b**. The excitation bands at 422, 560, and 608 nm for **Yb-1 a** and those at 419, 564, and 608 nm for **Yb-1 b** are identical to the respective UV/Vis absorptions, and this suggests that the excitation of the  $\text{Yb}^{3+}$  ion originates from the  $\pi \rightarrow \pi^*$  transitions of the porphyrinoid antennas.

Table 1 summarizes the important UV/Vis absorption and NIR photoluminescence data. All Yb complexes display an intense B (Soret) band in the 419–426 nm region and two Q bands in the 561–610 nm region. Close inspection of the ab-

sorptions for **Yb-1 a–5 a** reveals that the B and Q bands [Q(0,1), Q(0,0)] are systematically redshifted by 2–3, 9–17, and 15–17 nm, respectively, compared to the corresponding Yb porphyrins. More importantly, for Yb porpholactones **Yb-1 a–5 a**, the absorption intensity of the Q(0,0) band centered at 606–608 nm is about 8–12 times higher than that of Yb porphyrins **Yb-1 b–5 b**, whereas the Q(0,1) band showed lower intensity (ca. 0.6–0.7-fold) than those of the Yb porphyrins. The systematic redshifts and increasing extinction coefficients of the Q(0,0) band of Yb porpholactones **Yb-1 a–5 a** suggests perturbation of the energies of the frontier molecular orbitals of the porphyrin rings by the oxazolone moiety. All Yb complexes exhibit the typical near-IR emission centered at 972 nm arising from the  ${}^2F_{5/2} \rightarrow {}^2F_{7/2}$  transition of  $\text{Yb}^{3+}$ , which is split into multiple bands (1002, 1021 nm) by the ligand field. Weak visible emission was observed, and the emission band maxima are tabulated in Table 1. The emission at 600–720 nm originating from the singlet states of free bases is strongly reduced (by ca. 99%) in Yb complexes, due to intersystem crossing (ISC), which conveys the singlet excitation from the lowest  ${}^1\pi \rightarrow \pi^*$  state into the ligand triplet  ${}^3\pi \rightarrow \pi^*$  state.

To further illustrate the ligand effects on the NIR emission of Yb complexes, the quantum yields of NIR emission were measured by comparative methods<sup>[12,14]</sup> with YbTPP(Tp) (TPP = 5,10,15,20-tetraphenylporphyrinate, Tp = hydridotris(1-pyrazolyl)borate) as standard. The estimated error for the quantum yields is  $\pm 15\%$ .<sup>[14e]</sup> The quantum yields of the Yb porpholactones (2.4–4.1%) are 50–120% higher than those of the corresponding Yb porphyrins (Table 1). Besides  $\beta$ -lactonization of the porphyrins, the quantum yields of the  $\text{Yb}^{3+}$  complex are also dependent on the *meso* substituents; for example, **Yb-1 a** (3.3%) and **Yb-4 a** (4.1%) have higher quantum yields than the Yb porpholactones with other substituents. However, no systematic trend in electronic or steric effects on quantum yields was observed.

Luminescence lifetimes were recorded in order to evaluate the coordination environment around the  $\text{Yb}^{3+}$  cations in the complexes. The luminescence decays of the  $\text{Yb}^{3+}$  complexes in  $\text{CH}_2\text{Cl}_2$  were measured and fitted as double-exponential decays with lifetimes of 23.4–26.5  $\mu\text{s}$  (Table 1). This indicates that

a unique and consistent coordination environment is present around the Yb<sup>3+</sup> cation in the complexes. Interestingly, we found that, except for **Yb-4 a** and **Yb-4 b**, the lifetimes of Yb porpholactones are longer than those of the corresponding Yb porphyrins. The reason for the increased NIR emission lifetimes of Yb porpholactones due to introduction of the lactone moiety is not clear. Possible reasons are 1) the presence of an oxazolone moiety reduces the strength of the C–H oscillator in pyrrole moieties; 2) faster ISC after substitution with an oxazolone moiety results in increased population of the Yb excited state and longer NIR emission lifetimes.

### Phosphorescence in Gd complexes: comparison of triplet states of porphyrin and porpholactone

Since Yb porpholactones exhibited stronger NIR emission than the corresponding porphyrins, it is important to understand the mechanism of increased sensitization efficiency in Yb porpholactones. Assuming a porphyrin S<sub>1</sub>→porphyrinT<sub>1</sub>→Ln\* energy flow, the overall NIR emission efficiency  $\Phi_{\text{tot}}$  is regulated by the ISC efficiency (S<sub>1</sub>→T<sub>1</sub>,  $\Phi_{\text{ISC}}$ ), the energy-transfer efficiency (T<sub>1</sub>→Ln\*,  $\Phi_{\text{ET}}$ ), and the intrinsic Ln quantum yield (Ln\*→Ln,  $\Phi_{\text{Yb}} = \tau_{\text{obs}}/\tau_{\text{Yb}}$ ). The overall luminescence quantum yield  $\Phi_{\text{tot}}$  is the product of the yields of the three steps involved in producing photoluminescence [Eq. (1)]. The sensitization efficiency of porpholactone and porphyrin could be calculated according to Equation (2).

$$\Phi_{\text{tot}} = \Phi_{\text{ISC}} \Phi_{\text{ET}} \Phi_{\text{Yb}} \quad (1)$$

$$\eta_{\text{sen}} = \Phi_{\text{ISC}} \Phi_{\text{ET}} \quad (2)$$

Due to the difficulty of obtaining the radiative (or “natural”) lifetimes  $\tau_{\text{Yb}}$  in Yb porphyrin complexes, we assumed that the  $\tau_{\text{Yb}}$  values of porphyrins and porpholactones are similar because of their similar coordination spheres. Thus, the relative sensitization efficiency of porpholactone and porphyrin  $\eta_{\text{Yb-a}}/\eta_{\text{Yb-b}}$  was estimated according to Equations (1) and (2). From the lifetimes of NIR emission collected in Table 1, we found that the longer lifetimes of Yb porpholactones may increase the metal-based quantum yields  $\Phi_{\text{Yb}}$  ( $\tau_{\text{obs}}/\tau_{\text{Yb}}$ ). Thus, the relative sensitization ability could be deduced from Equation (2). Systematic increases (33–99%) in sensitization ability of Yb porpholactones compared with their corresponding Yb porphyrins were calculated (Table 1). It is noteworthy that the relative sensitization efficiency is also affected by the substituents of the *meso*-phenyl groups, but no systematic trend was observed.

To investigate the role of the triplet state in sensitization efficiency,<sup>[15]</sup> we estimated the ligand triplet levels in Gd porphyrin and porpholactone. Because the emitting levels of the Gd<sup>3+</sup> ion are of higher energy than the ligand singlet and triplet states, the lack of energy transfer would prevent depletion of the ligand triplet state and allow the emission of phosphorescence. Figure 2 shows the emission from **Gd-1 a** and **Gd-1 b** on excitation at 420 nm, which is masked at room temperature, at 77 K in methanol/ethanol (1/1). In the range of 730–900 nm,

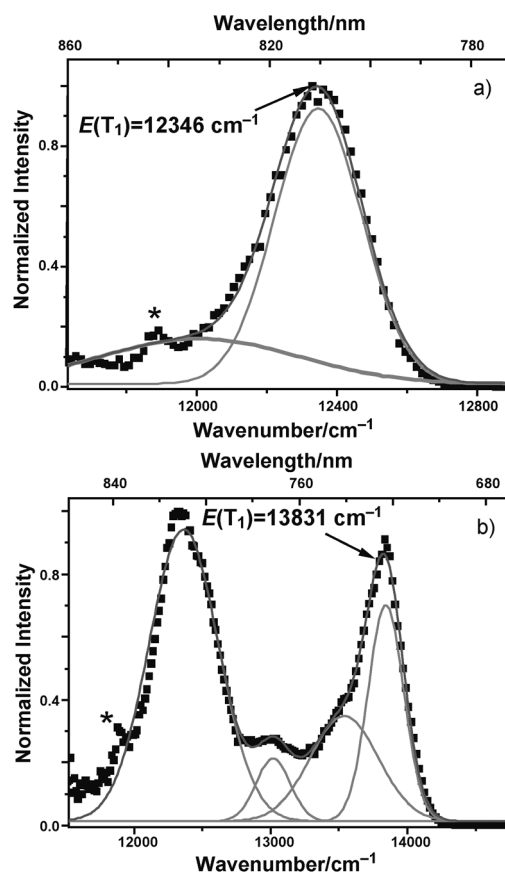
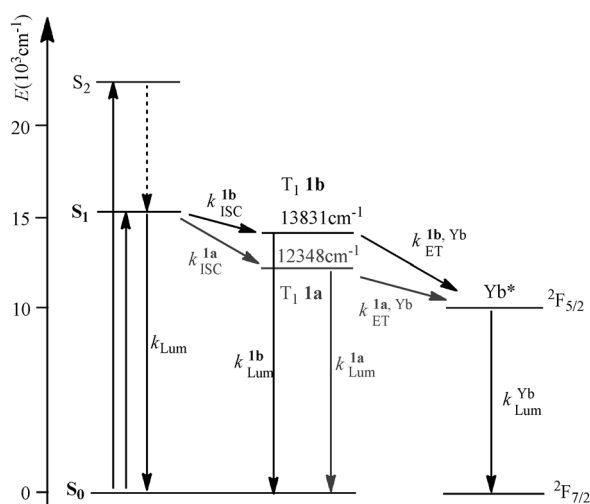


**Figure 2.** Low-temperature (77 K) emission spectra ( $\lambda_{\text{ex}} = 420$  nm) of a) **Gd-1 a** and b) **Gd-1 b** in MeOH/EtOH (1/1), with cumulative fit function and individual Gaussians in gray. The asterisk indicates a second-order transmission of the 420 nm excitation.

**Gd-1 a** emits at 810 nm, and **Gd-1 b** at 723, 770, and 809 nm. The triplet experimental decay times of 51.8  $\mu\text{s}$  for **Gd-1 a** and 130.1  $\mu\text{s}$  for **Gd-1 b** confirm the observation of phosphorescence. The redshifted phosphorescence and shorter lifetime for **Gd-1 a** are consistent with those of previously reported Pd and Pt porpholactones.<sup>[9]</sup> The lowest-energy zero-phonon ( $\nu_{0-0}$ ) band of the triplet state was estimated by spectral deconvolution of the luminescence signal into a series of overlapping Gaussian functions, which yielded values of 12346 and 13831  $\text{cm}^{-1}$  for the lowest-energy T<sub>1</sub> states of **1 a** and **1 b**, respectively. This clearly suggests that replacement of an oxazolone moiety markedly lowers the excited T<sub>1</sub> state ( $\Delta E = 1485$   $\text{cm}^{-1}$ ). According to the energy-gap law, the probability of intramolecular energy transfer between two electronic states is inversely proportional to their energy difference.<sup>[16]</sup> Thus, as shown in Scheme 2, **Yb-1 a** has a narrower energy gap ( $\Delta E = 2546$   $\text{cm}^{-1}$ ) between the porphyrinoid T<sub>1</sub> state and the lowest excited states of Yb<sup>3+</sup> than **Yb-1 b** ( $\Delta E = 4031$   $\text{cm}^{-1}$ ), which indicates more efficient energy transfer ( $\Phi_{\text{ET}}$ ) from **1 a** to Yb<sup>3+</sup>.

$\beta$ -Lactonization of porphyrins affects the electronic structure. Iterative extended Hückel calculations by Gouterman and co-workers suggested a porphyrinic electronic structure with the  $\pi$  orbitals on both the oxa and oxo oxygen atoms present in



**Scheme 2.** Proposed energy-transfer diagram between porphyrinoids **1a**, **1b** and  $\text{Yb}^{\text{III}}$  ion.

three of the four porphyrin orbitals and a resulting symmetry change.<sup>[5b,d]</sup> This perturbation of the molecular orbitals of the lactone moiety would result in changes in the HOMO, LUMO, and LUMO + 1 of the porphyrin, which correspond to  $S_0$ ,  $S_1$ , and  $S_2$  levels, respectively. Since the electron-withdrawing lactone moiety would stabilize HOMO or HOMO−1 more than LUMO and LUMO + 1, it is not surprising that in **Yb-1a** the Q(0,0) band, which is assigned to  $S_0$ – $S_1$  transitions, is redshifted by 26 nm and the  $T_1$  state is lower in energy ( $\Delta E = 2546 \text{ cm}^{-1}$ ) compared to **Yb-1b**. This indicates a smaller energy gap between the  $T_1$  state of the porphyrinic ligand and the lowest excited state of  $\text{Yb}^{3+}$ .

### Transient absorption spectra of **Yb-1a** and **Yb-1b**

To provide additional information on the electronic structure and lifetime of the emitting states, transient absorption (TA) spectroscopy was carried out on **Yb-1a** and **Yb-1b**. TA spectra for **Yb-1a** and **Yb-1b** in  $\text{CH}_2\text{Cl}_2$  were recorded at various delay times following excitation by a 420 nm laser pulse (10 Hz, 2 mJ per pulse). As shown in Figure 3a, the TA difference spectra for **Yb-1a** and **Yb-1b** (see Figure S28 in the Supporting Information) over the 400–650 nm region coincide with the Soret and Q-band ground state. **Yb-1a** and **Yb-1b** show a bleaching of the Soret band at 421 and 418 nm and net absorption around 409 and 406 nm. The transient lifetimes for the  $\text{Yb}^{\text{III}}$  porphyrin complexes at the Soret band are  $\tau = 30.8$  and  $17.0 \mu\text{s}$ . The Q-band region shows a derivative-shaped transient absorption. Weak transient absorption (bleaching) was observed at the Q bands for **Yb-1a** and **Yb-1b**, and the transient lifetimes were difficult to obtain owing to the low absorption intensity. Transient absorptions of **Yb-1a** and **Yb-1b** are also similar in profile and lifetime to those of  $\text{Yb}^{\text{III}}$  porphyrin analogues.<sup>[3c]</sup> In all cases, coordination of a lanthanide to porphyrin or porpholactone results in rapid ISC of the  $S_0 \rightarrow T_1$  state followed by energy transfer to the lanthanide. For **Yb-1a** and **Yb-1b**,  $\text{Yb}^{3+}$  in their respective excited states may simply be exerting a different

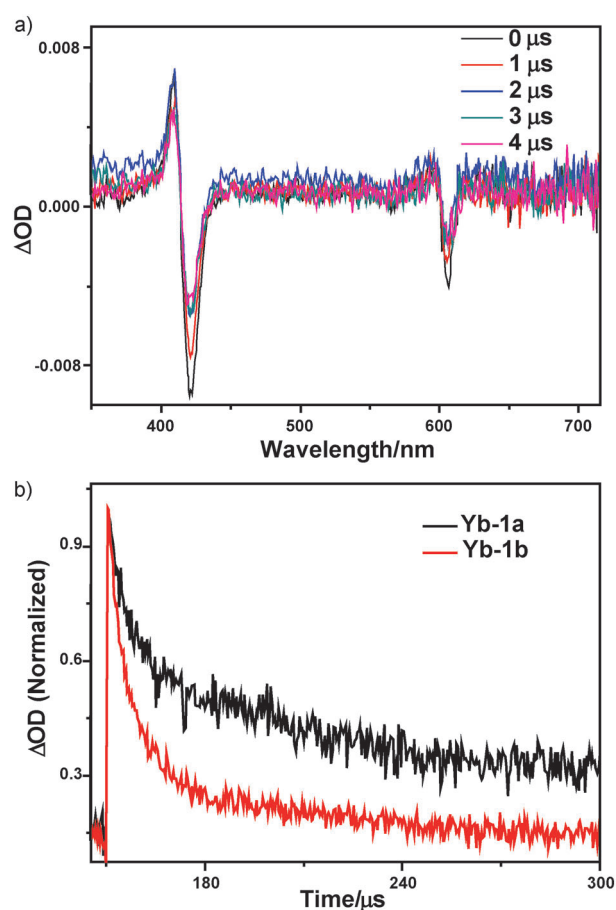
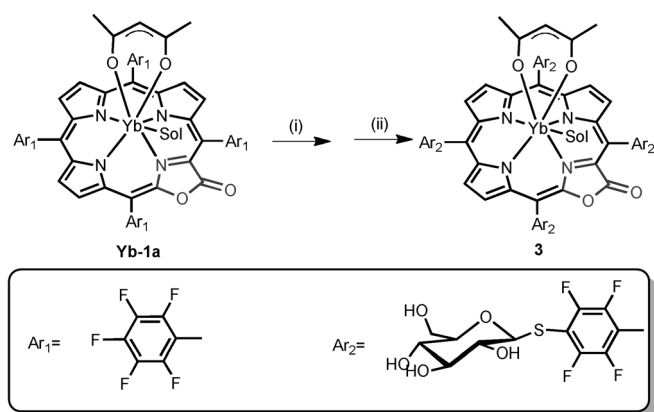


**Figure 3.** a) Transient absorption spectra of **Yb-1a** in  $\text{CH}_2\text{Cl}_2$  solution. Spectra were obtained at several delay times following the 420 nm laser excitation pulse (10 Hz, 2 mJ per pulse). b) Transient decay curves of **Yb-1a** and **Yb-1b** in  $\text{CH}_2\text{Cl}_2$ , monitored at 408 nm.

electronic influence on the  $\pi$ -electron system of the porphyrinoids, which would account for a shift in the absorption of the excited lanthanide complexes. According to Equation (1), enhanced lifetime due to  $\beta$ -lactonization of porphyrinic ligands may increase the intrinsic Ln quantum yield ( $\text{Ln}^* \rightarrow \text{Ln}$ ,  $\Phi_{\text{Yb}} = \tau_{\text{obs}}/\tau_{\text{Yb}}$ ), which is an important factor in the overall NIR emission efficiency ( $\Phi_{\text{tot}}$ ).

### **Yb porpholactone as a NIR-emissive bioprobe in aqueous media**

To demonstrate the potential applications of Yb porphyrinoids, we investigated the ability to detect biological analytes in the NIR emission window of 900–1100 nm, which has less interference from both light scattering and autofluorescence of biological matter. Because Yb porpholactones display higher NIR luminescence than the Yb porphyrin analogues, we chose **Yb-1a** and attached a glucose moiety through substitution of *para*-F atoms to make it water-soluble. As shown in Scheme 3, direct reaction of **Yb-1a** with 2,3,4,6-tetra-*O*-acetylglucosyl thioacetate followed by subsequent hydrolysis of the acetyl group by NaOMe afforded glycosylated ytterbium porpholactone **3** in 40% yield. Complex **3** was characterized by matrix-



**Scheme 3.** Synthetic route for **3**. i) 2,3,4,6-tetra-*O*-acetylglucosyl thioacetate, DMF/HNEt<sub>2</sub> (10/1); ii) CH<sub>3</sub>ONa, CH<sub>2</sub>Cl<sub>2</sub>/MeOH (1/1).

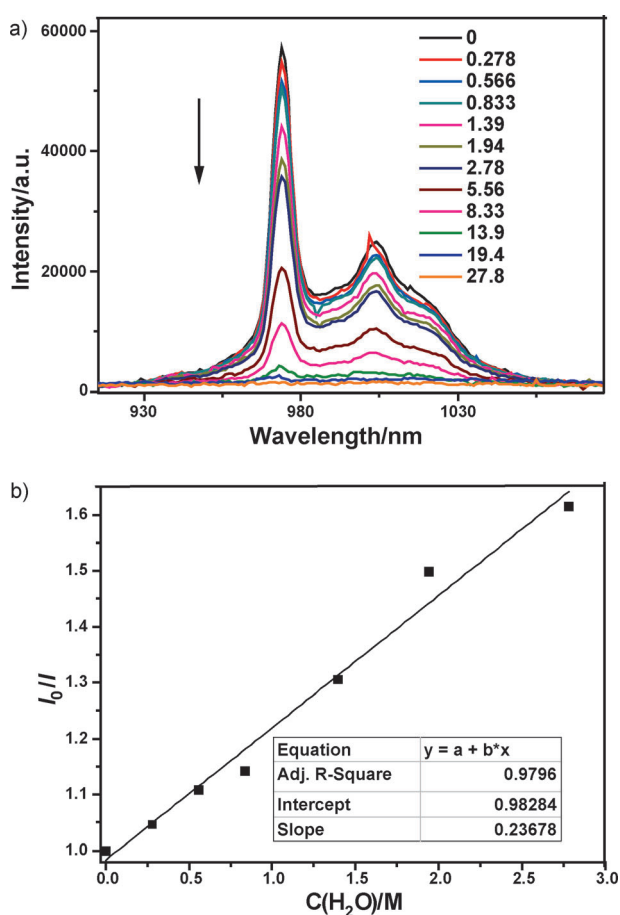


**Figure 4.** a) NIR emission spectral changes of **3** versus concentration of H<sub>2</sub>O in DMSO. b) Stern–Volmer plot of NIR emission intensity at 975 nm for quenching of **3** with H<sub>2</sub>O.

assisted laser desorption ionization time-of-flight mass spectrometry (MALDI-TOF MS) and UV/Vis and IR spectroscopy.

We then examined the effect of water on the NIR emission of **3**. On addition of water, the NIR emission at 900–1100 nm was quenched gradually, as shown in Figure 4a. Comparison of the luminescence lifetimes in H<sub>2</sub>O (0.5% DMSO, 3.9 μs) and

D<sub>2</sub>O (0.5% DMSO, 12.1 μs) can be used to quantify the number of solvent molecules coordinated to the lanthanide cations. The hydration/solvation number was obtained by using empirical Equation (3), which was developed by Beeby et al.<sup>[17]</sup>

$$q = A(k_H - k_D - B) \quad A = 1.0 \mu\text{s}, B = 0.2 \mu\text{s}^{-1} \quad (3)$$

where  $q$  is the number of water molecules bound to the Yb<sup>3+</sup> ion in the first coordination sphere,  $k_H$  and  $k_D$  are the rate constants of excited states of lanthanide ion in H<sub>2</sub>O and D<sub>2</sub>O, respectively,  $A$  is a proportionality constant related to the sensitivity of the Yb<sup>3+</sup> ion to vibrational quenching by O–H oscillators, and  $B$  is a correction factor for outer-sphere water molecules.

By applying this formula,  $q$  values of  $-0.03$  were calculated for the Yb<sup>III</sup> complexes. These near-zero values indicate that no water molecules are bound to the lanthanide ion in the first coordination sphere of the complexes in solution. We assumed that the vacant site of the Yb<sup>3+</sup> cation might be occupied by DMSO. Therefore, we can conclude that the nonradiative deactivation of the NIR emission of **3** was due to outer-sphere water molecules. This was confirmed by a Stern–Volmer (SV) plot of the NIR emission from **3** quenched with H<sub>2</sub>O (0–2.78 M). As shown in Figure 4b, the overall quenching constant  $K_{SV}$  was 0.24 M<sup>-1</sup>. Considering that  $K_{SV} = k_q \tau$ , where  $\tau$  is the lifetime of the excited chromophore in the absence of quencher (23.3 μs), we calculated the bimolecular quenching constant  $k_q$  to be 1.0 × 10<sup>4</sup> M<sup>-1</sup> s<sup>-1</sup>, which is much lower than the corresponding value of diffusion-limited quenching (10<sup>10</sup> M<sup>-1</sup> s<sup>-1</sup>). Thus, the quenching process could be assigned to a dynamic quenching process,<sup>[18]</sup> which indicates that the binding affinity of water towards the Yb center was very weak. Therefore, quenching of the NIR luminescence process may be caused by collision between the outer-sphere water molecules and the Yb center.

Glucose conjugate **3** was then applied in detecting glucose-binding proteins such as glucose oxidase (GOx) by means of fluorescence spectroscopic measurements. Solutions of GOx with concentrations increasing in steps of about 0.08 μM were mixed with a 4 μM solution of **3** in Tris-HCl buffer (50 mM, pH 7.4). The NIR emission at 900–1100 nm increased with increasing GOx concentration (Figure 5a) up to a GOx concentration of 1.25 μM, above which the emission intensity remained constant at approximately 18 times the initial emission intensity in the absence of GOx. The lifetime of NIR emission was 8.1 μs, which is twice that of **3** in aqueous medium. This suggested that the NIR emission of **3** could be switched on by the glucose-binding protein GOx in aqueous medium. To examine the specificity of switched-on NIR emission, we chose 12 other proteins: avidin, cytochrome c, concanavalin A (con A), deoxyribonuclease I (DNase I), ribonuclease A (RNase A), lysozyme, immunoglobulin G (Ig G), papain, trypsin, bovine serum albumin (BSA), human serum albumin (HSA) and phytohemagglutinin (PHA). As shown in Figure 5b, only GOx showed an obvious increase in emission intensity compared to the other 12 proteins at the same concentration. These results suggested that the switched-on emission is a specific response to GOx and may

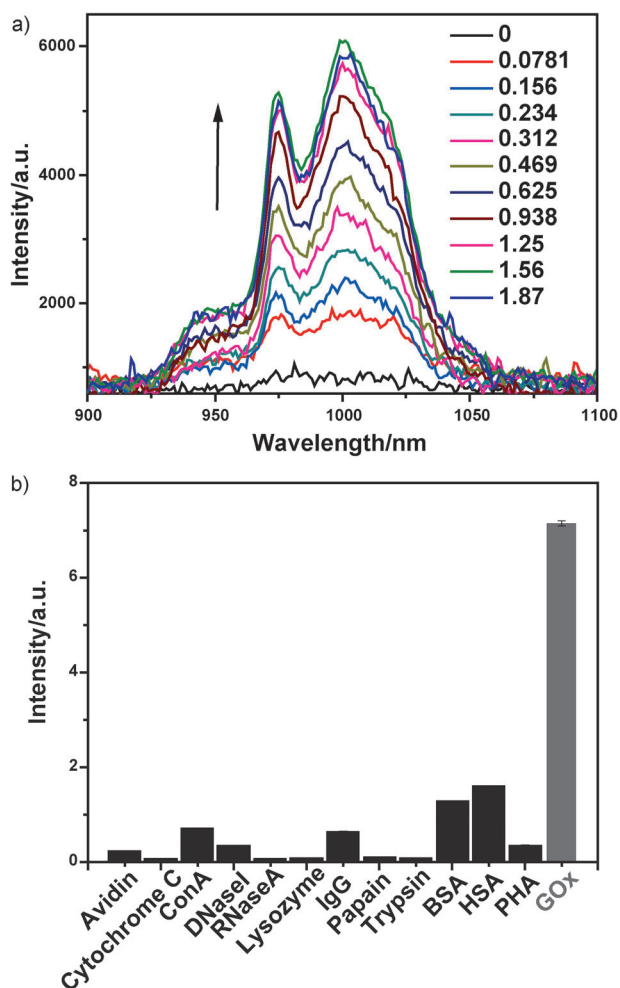


**Figure 5.** a) NIR emission spectra of **3** (4 μM) at various concentrations [μM] of GOx in Tris-HCl buffer (50 mM, pH 7.4) at 25 °C. b) NIR emission intensity per mole of protein for **3** (4 μM) treated with 13 different proteins (1 mg mL<sup>-1</sup>) in Tris-HCl buffer (50 mM, pH 7.4) at 25 °C; intensity monitored at 975 nm.

be due to binding of the glucose conjugate to the glucose-binding site of GOx.

To verify this, we added free glucose progressively to the mixed solution of **3** and GOx in Tris-HCl buffer (50 mM, pH 7.4, containing 1.25 μM GOx). If the glucose conjugate of **3** occupied the glucose binding site, the competition between **3** and free glucose would result dissociation of **3** from GOx and thus quenching of the NIR emission. As shown in Figure 6, we observed decreased NIR emission with increasing amount of glucose. To further demonstrate the specificity for glucose, we investigated the sugars fructose, galactose, mannose, xylose, lactose, and sucrose in competition with **3** and found that only addition of glucose efficiently quenched the NIR emission of **3** (Figure 6, inset). Although the recognition of glucose at the side of the molecule bearing the anomeric carbon atom is well known,<sup>[19]</sup> in this work, the GOx-recognition mechanism of the modified glucose moiety is not clear. In addition, we carried out transient absorption measurements on **3** in aqueous medium (Figure S32 in the Supporting Information), on bind-

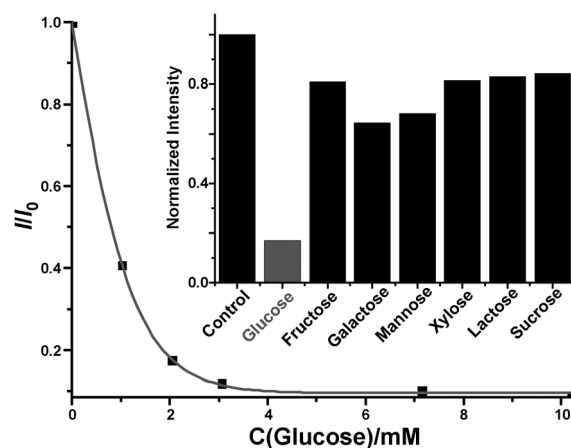


**Figure 6.** Relative NIR emission intensity at 975 nm of **3** (4 μM) versus concentration of glucose in the presence of GOx (1.25 μM) in Tris-HCl buffer (50 mM, pH 7.4) at 25 °C. Inset: Relative NIR emission intensity monitored at 975 nm of **3** (4 μM) treated with seven different sugars (2 mM) in the presence of GOx (1.25 μM) in Tris-HCl buffer (50 mM, pH 7.4) at 25 °C.

ing of **3** with GOx (Figure S34 in the Supporting Information), and for the addition of glucose to a solution of **3** and GOx (Figure S36 in the Supporting Information). Although the resolution of the spectra was not good, transient decay lifetimes of 0.3, 2.9 and 1.4 μs, respectively were measured at 430 nm (Figures S33, S35, and S37 in the Supporting Information); this suggests that changes in GOx and glucose affect the photophysical properties of **3** in Tris-HCl buffer. These results strongly suggest that complex **3** binds to the glucose-binding site of GOx and thus enhances the NIR emission by protecting Yb<sup>3+</sup> cations against nonradiative deactivation induced by water.

## Conclusion

We have described the synthesis and photophysical properties of Yb porpholactones. Through comparative studies with Yb porphyrins, we found that β-lactonization of porphyrin ligands enhances the sensitization efficiency of the NIR luminescence of Yb<sup>3+</sup> by narrowing the energy gap between the porphyrinoid T<sub>1</sub> state and the lowest excited states of Yb<sup>3+</sup> and increasing the NIR emission lifetime. Thus, this work has demonstrated the importance of β-modification of the porphyrin periphery or tuning the molecular symmetry in increasing the NIR sensitization efficiency of lanthanides and may aid in the design of further efficient NIR-emissive lanthanide complexes. Moreover, by glycosylation of ytterbium complex **3**, we demonstrated its potential application as a switchable probe emitting in the NIR region of 900–1100 nm. The emission could be switched on and off in the sequence “off (in water)→on (with GOx)→off (with glucose)”, which provides access to further development of Ln porphyrinates as NIR-emissive probes in the region in which biological tissues and fluids are relatively transparent.

## Experimental Section

Unless otherwise stated, all reactions were performed under an inert atmosphere of nitrogen by using standard Schlenk techniques and flame-dried flasks. UV/Vis spectra were recorded on an Agilent 8453 UV/Vis spectrometer equipped with an Agilent 89090A thermostat ( $\pm 0.1$  °C). The emission spectrum and lifetime were recorded on an Edinburgh Analytical Instruments FLS920 lifetime and steady-state spectrometer (450 W Xe lamp/microsecond flash lamp, PMT R928 for visible emission spectrum, Ge detector for NIR emission spectrum, Hamamatsu R5509-73 PMT with C9940-02 cooler for NIR luminescence lifetime). Nanosecond transient absorption measurements were performed on an LP-920 laser flash photolysis setup (Edinburgh) with a computer-controlled Nd:YAG laser/OPO system from Opotek (Vibrant 355 II). Mass spectra were recorded on Bruker APEX IV FT-ICR mass spectrometer (ESI-MS) or Biosystems 4700 Proteomics Analyzer 283 (MALDI-TOF MS). Elemental analyses (C, H, N) were recorded on Elementar Analysensysteme GmbH vario EL Elemental Analyzer.  $^1\text{H}$  NMR spectra were recorded on a Varian Mercury Plus 300 MHz spectrophotometer. IR spectra were recorded on a Bruker VECTOR22 FTIR spectrometer as KBr pellets. For the optical measurements in liquid solution, spectroscopic-grade DMSO and  $\text{CH}_2\text{Cl}_2$  were used as purchased from Alfa-Aesar and anhydrous  $\text{CH}_2\text{Cl}_2$  was distilled from calcium hydride. Optical measurements at 77 K were performed in methanol/ethanol (1/1) glass-forming solvent mixture.

**Synthesis of Yb-1 a:** Porpholactones were prepared according to our modified procedure.<sup>[5f]</sup> **Yb-1 a** was prepared according to a procedure similar to that described in the literature.<sup>[3a]</sup> 5,10,15,20-Tetra(pentafluorophenyl)porpholactone (**1 a**; 50 mg, 0.05 mmol) and  $\text{Yb}(\text{acac})_3 \cdot 3\text{H}_2\text{O}$  (80 mg, 0.15 mmol) were added to a Schlenk tube, and then 5 mL of 1,2,4-trichlorobenzene (TCB) was added. The mixture was heated at reflux for 8 h. The color of the reaction mixture changed from red-purple to blue-purple. After cooling to room temperature, the reaction mixture was transferred to a silica column. TCB was first eluted with petroleum ether, then unconsumed free-base porpholactone with  $\text{CH}_2\text{Cl}_2$ , and finally the product with  $\text{CH}_2\text{Cl}_2/\text{MeOH}$  (5/1). The product was recrystallized from *n*-hexane/ $\text{CH}_2\text{Cl}_2$  as a blue-purple solid. M.p.  $> 300$  °C (decomp); yield: 86% (54 mg); IR (KBr):  $\tilde{\nu} = 1778\text{ cm}^{-1}$  (C=O); HRMS (ESI<sup>+</sup>):  $m/z$  calcd for  $\text{C}_{48}\text{H}_{15}\text{F}_{20}\text{KN}_4\text{O}_5\text{Yb}$  [ $M+\text{H}_2\text{O}+\text{K}$ ]<sup>+</sup>: 1319.9749; found: 1319.9863; elemental analysis calcd (%) for  $\text{C}_{48}\text{H}_{15}\text{F}_{20}\text{N}_4\text{O}_4\text{Yb} + \text{CH}_3\text{OH} + 2\text{H}_2\text{O}$ : C 44.23, H 1.59, N 4.21; found: C 44.29, H 1.62, N 4.24.

**Synthesis of Yb-1 b:** **Yb-1 b** was prepared according to a procedure similar to that of **Yb-1 a** as a red-purple solid. M.p.  $> 300$  °C (decomp); yield: 78% (49 mg); HRMS (ESI<sup>+</sup>):  $m/z$  calcd for  $\text{C}_{50}\text{H}_{24}\text{F}_{20}\text{N}_4\text{O}_5\text{Yb}$  [ $M+\text{CH}_3\text{OH}+2\text{H}_2\text{O}+\text{H}$ ]<sup>+</sup>: 1314.0824; found: 1314.1098; elemental analysis calcd (%) for  $\text{C}_{49}\text{H}_{13}\text{F}_{20}\text{N}_4\text{O}_2\text{Yb} + \text{CH}_3\text{OH} + \text{H}_2\text{O}$ : C 46.38, H 1.63, N 4.33; found: C 47.07, H 1.83, N 4.72.

**Synthesis of Yb-2 a:** **Yb-2 a** was prepared according to a procedure similar to that of **Yb-1 a** as a blue purple solid. M.p.  $> 300$  °C (decomp); yield: 33% (15 mg); IR (KBr):  $\tilde{\nu} = 1759\text{ cm}^{-1}$  (C=O); HRMS (ESI<sup>+</sup>):  $m/z$  calcd for  $\text{C}_{48}\text{H}_{35}\text{KN}_4\text{O}_5\text{Yb}$  [ $M+\text{H}_2\text{O}+\text{K}$ ]<sup>+</sup>: 960.1633; found: 960.1742; elemental analysis calcd (%) for  $\text{C}_{48}\text{H}_{33}\text{N}_4\text{O}_4\text{Yb} + \text{CH}_3\text{OH} + \text{H}_2\text{O}$ : C 61.76, H 4.13, N 5.88; found: C 61.76, H 4.12, N 5.59.

**Synthesis of Yb-2 b:** **Yb-2 b** was prepared according to a procedure similar to that of **Yb-1 a** as a red purple solid. M.p.  $> 300$  °C (decomp); yield: 35% (15 mg); HRMS (ESI<sup>+</sup>):  $m/z$  calcd for  $\text{C}_{45}\text{H}_{32}\text{N}_4\text{OYb}$  818.1973: [ $M-\text{acac}+\text{CH}_3\text{OH}$ ]<sup>+</sup>; found: 818.1923; elemental analysis calcd (%) for  $\text{C}_{49}\text{H}_{35}\text{N}_4\text{O}_2\text{Yb} + 2\text{H}_2\text{O}$ : C 63.91, H 4.27, N 6.08; found: C 63.69, H 4.17, N 6.18.

**Synthesis of Yb-3 a:** **Yb-3 a** was prepared according to a procedure similar to that of **Yb-1 a** as a blue-purple solid. M.p.  $> 300$  °C (decomp); yield: 41% (21 mg); IR (KBr):  $\tilde{\nu} = 1772\text{ cm}^{-1}$  (C=O); HRMS (ESI<sup>+</sup>):  $m/z$  calcd for  $\text{C}_{48}\text{H}_{31}\text{Cl}_4\text{KN}_4\text{O}_5\text{Yb}$  [ $M+\text{H}_2\text{O}+\text{K}$ ]<sup>+</sup>: 1098.0045; found: 1098.0110; elemental analysis calcd (%) for  $\text{C}_{48}\text{H}_{29}\text{Cl}_4\text{N}_4\text{O}_4\text{Yb} + 0.5\text{H}_2\text{O} + 1.5\text{CH}_3\text{OH}$ : C 54.16, H 3.31, N 5.10; found: C 54.21, H 3.09, N 4.86.

**Synthesis of Yb-3 b:** **Yb-3 b** was prepared according to a procedure similar to that of **Yb-1 a** as red-purple solid. M.p.  $> 300$  °C (decomp); yield: 58% (30 mg); HRMS (ESI<sup>+</sup>):  $m/z$  calcd for  $\text{C}_{49}\text{H}_{33}\text{Cl}_4\text{KN}_4\text{O}_3\text{Yb}$  [ $M+\text{H}_2\text{O}+\text{K}$ ]<sup>+</sup>: 1080.0303; found: 1080.0392; elemental analysis calcd (%) for  $\text{C}_{49}\text{H}_{31}\text{Cl}_4\text{N}_4\text{O}_2\text{Yb} + 2\text{H}_2\text{O}$ : C 55.59, H 3.33, N 5.29; found: C 55.67, H 3.38, N 5.15.

**Synthesis of Yb-4 a:** **Yb-4 a** was prepared according to a procedure similar to that of **Yb-1 a** as a blue-purple solid. M.p.  $> 300$  °C (decomp); yield: 80% (47 mg); IR (KBr):  $\tilde{\nu} = 1769\text{ cm}^{-1}$  (C=O); HRMS (ESI<sup>+</sup>):  $m/z$  calcd for  $\text{C}_{52}\text{H}_{31}\text{F}_{12}\text{KN}_4\text{O}_5\text{Yb}$  [ $M+\text{H}_2\text{O}+\text{K}$ ]<sup>+</sup>: 1232.1128; found: 1232.1194; elemental analysis calcd (%) for  $\text{C}_{52}\text{H}_{29}\text{F}_{12}\text{N}_4\text{O}_4\text{Yb} + 0.8\text{CH}_3\text{OH} + \text{C}_6\text{H}_{14}$  (*n*-hexane): C 54.97, H 3.47, N 4.36; found: C 54.24, H 3.24, N 4.14.

**Synthesis of Yb-4 b:** **Yb-4 b** was prepared according to a procedure similar to that of **Yb-1 a** as a red-purple solid. M.p.  $> 300$  °C (decomp); yield: 85% (49 mg); HRMS (ESI<sup>+</sup>):  $m/z$  calcd for  $\text{C}_{53}\text{H}_{33}\text{F}_{12}\text{KN}_4\text{O}_3\text{Yb}$  [ $M+\text{H}_2\text{O}+\text{K}$ ]<sup>+</sup>: 1214.1387; found: 1214.1482; elemental analysis calcd (%) for  $\text{C}_{53}\text{H}_{31}\text{F}_{12}\text{N}_4\text{O}_2\text{Yb} + 0.8\text{CH}_3\text{OH} + \text{C}_6\text{H}_{14}$  (*n*-hexane): C 56.70, H 3.68, N 4.42; found: C 56.80, H 3.67, N 4.11.

**Synthesis of Yb-5 a:** **Yb-5 a** was prepared according to the procedure for **Yb-1 a** with modifications. 5,10,15,20-Tetramesitylporpholactone (**5 a**; 40 mg, 0.05 mmol),  $\text{Yb}(\text{acac})_3 \cdot 3\text{H}_2\text{O}$  (80 mg, 0.15 mmol), and NaH (12 mg, 0.5 mmol) were added to a Schlenk tube, and then TCB (5 mL) was added. The mixture was heated at reflux for 12 h. The color of the reaction mixture changed from red-purple to blue-purple. After cooling to room temperature, the reaction mixture was transferred to a silica column. TCB was first eluted with petroleum ether, then unconsumed free-base porpholactone with  $\text{CH}_2\text{Cl}_2$ , and finally the product with  $\text{CH}_2\text{Cl}_2/\text{MeOH}$  (5/1). The product was recrystallized from *n*-hexane/ $\text{CH}_2\text{Cl}_2$  as a blue-purple solid. M.p.  $> 300$  °C (decomp); yield: 45% (24 mg); IR (KBr):  $\tilde{\nu} = 1761\text{ cm}^{-1}$  (C=O); HRMS (ESI<sup>+</sup>):  $m/z$  calcd for  $\text{C}_{60}\text{H}_{58}\text{N}_4\text{O}_4\text{Yb}$  [ $M+\text{H}$ ]<sup>+</sup>: 1072.3847; found: 1072.3796; elemental analysis calcd (%) for  $\text{C}_{60}\text{H}_57\text{N}_4\text{O}_4\text{Yb} + \text{H}_2\text{O} + \text{CH}_3\text{OH} + \text{C}_6\text{H}_{14}$  (*n*-hexane): C 66.76, H 6.27, N 4.65; found: C 66.71, H 6.53, N 4.59.

**Synthesis of Yb-5 b:** **Yb-5 b** was prepared according to a procedure similar to that of **Yb-5 a** as a red-purple solid. M.p.  $> 300$  °C (decomp); yield: 58% (31 mg); HRMS (ESI<sup>+</sup>):  $m/z$  calcd for  $\text{C}_{61}\text{H}_{60}\text{N}_4\text{O}_2\text{Yb}$  [ $M+\text{H}$ ]<sup>+</sup>: 1054.4105; found: 1054.4010. elemental analysis calcd (%) for  $\text{C}_{61}\text{H}_{59}\text{N}_4\text{O}_2\text{Yb} + \text{H}_2\text{O} + \text{CH}_3\text{OH} + \text{C}_6\text{H}_{12}$  (*n*-hexane): C 68.78, H 6.54, N 4.72; found: C 68.43, H 6.07, N 4.93.

**Synthesis of YbTPP(Tp):** YbTPP(Tp) was synthesized according to the literature.<sup>[20]</sup> HRMS (ESI<sup>+</sup>):  $m/z$  calcd for  $\text{C}_{53}\text{H}_{39}\text{BN}_{10}\text{Yb}$  [ $M+\text{H}$ ]<sup>+</sup>: 1000.2841; found: 1000.2843; elemental analysis calcd (%) for  $\text{C}_{53}\text{H}_{39}\text{BN}_{10}\text{Yb}$ : C 63.73, H 3.83, N 14.02; found: C 63.54, H 3.87, N 13.72. For  $^1\text{H}$  NMR spectrum, see Figure S45 in the Supporting Information.

**Synthesis of Gd-1 a:** **Gd-1 a** was prepared according to a procedure similar to that of **Yb-1 a** as a blue-purple solid. M.p.  $> 300$  °C (decomp); yield: 85% (53 mg), IR (KBr):  $\tilde{\nu} = 1770\text{ cm}^{-1}$  (C=O). HRMS (ESI<sup>+</sup>):  $m/z$  calcd for  $\text{C}_{48}\text{H}_{15}\text{F}_{20}\text{KN}_4\text{O}_5\text{Gd}$  [ $M+\text{H}_2\text{O}+\text{K}$ ]<sup>+</sup>: 1303.9601; found: 1303.9626; elemental analysis calcd (%) for  $\text{C}_{48}\text{H}_{13}\text{F}_{20}\text{GdN}_4\text{O}_4 + 2.5\text{CH}_3\text{OH}$ : C 45.71, H 1.75, N 4.22; found: C 46.22, H 1.82, N 4.20.

**Synthesis of Gd-1 b:** Gd-1 b was prepared according to a procedure similar to that of Yb-1 a as a red-purple solid. M.p. > 300 °C (decomp); yield: 82 % (50 mg); HRMS (ESI<sup>+</sup>): *m/z* calcd for C<sub>49</sub>H<sub>17</sub>F<sub>20</sub>KN<sub>4</sub>O<sub>3</sub>Gd [M+H<sub>2</sub>O+K]<sup>+</sup>: 1285.9859; found: 1285.9901; elemental analysis calcd (%) for C<sub>49</sub>H<sub>15</sub>F<sub>20</sub>GdN<sub>4</sub>O<sub>2</sub>+3CH<sub>3</sub>OH: C 47.14, H 2.05, N 4.23; found: C 49.83, H 2.10, N 4.81.

**Synthesis of 3:** Complex 3 was prepared according to a procedure similar to that described in the literature.<sup>[21]</sup> Yb-1 a (33.0 mg, 25 μmol) and 2,3,4,6-tetra-*O*-acetylglucosyl thioacetate (87.0 mg, 200 μmol) were dissolved in 10 mL of DMF and 1 mL of diethylamine. The solution was stirred for 8 h at room temperature. The solvent was evaporated under reduced pressure and the product purified by column chromatography with CH<sub>2</sub>Cl<sub>2</sub>/MeOH (16/1) as eluent to give a deep purple product. The product was dissolved in CH<sub>2</sub>Cl<sub>2</sub>/MeOH (1/1) without characterization and treated with 16 equivalents of CH<sub>3</sub>ONa at room temperature for 4 h. The mixture was filtered and the product purified by column chromatography on silica to give the product as a blue purple solid. Yield: 40%; IR (KBr):  $\tilde{\nu}$  = 1760 cm<sup>-1</sup> (C=O); MS (MALDI<sup>+</sup>, DMF): *m/z* calcd for C<sub>75</sub>H<sub>64</sub>F<sub>16</sub>KN<sub>5</sub>O<sub>25</sub>S<sub>4</sub>Yb [M+DMF+K]<sup>+</sup>: 2079.2; found: 2079.1.

**Transient absorption:** Excitation at 420 nm with a power of 2.0 mJ per pulse from a computer-controlled Nd:YAG laser/OPO system operating at 10 Hz was directed to the sample with an optical absorbance of 0.6 at the excitation wavelength. The laser and analyzing light beam passed perpendicularly through a 1 cm quartz cell. The complete time-resolved spectra were obtained by using a gated CCD camera (Andor iSTAR); the kinetic traces were detected by a Tektronix TDS 3012B oscilloscope and a R928P photomultiplier and analyzed by Edinburgh analytical software (LP920).

**Determination of quantum yields:** Quantum yields in solution were determined by comparative method<sup>[12,14]</sup> and the equation:  $\Phi_s/\Phi_r = (G_s/G_r)(\eta_s^2/\eta_r^2)$ , where the subscripts r and s denote reference and sample, respectively,  $\Phi$  is the quantum yield,  $G$  the slope of the plot of integrated emission intensity versus absorbance, and  $\eta$  the refractive index of the solvent. The reference was YbTPP(Tp) in CH<sub>2</sub>Cl<sub>2</sub> ( $\Phi = 0.032$ ,<sup>[3c,12]</sup>  $\lambda_{ex} = 425$  nm). Because of the low absorption of Yb-1 a and Yb-1 b at 425 nm, we also performed measurements at 420 nm. YbTPP(Tp) solutions with five different concentrations were first prepared in anhydrous CH<sub>2</sub>Cl<sub>2</sub>, the absorbance of the solutions at 420 and 425 nm were recorded on an Agilent 8453 UV/Vis spectrometer equipped with an Agilent 89090A thermostat ( $\pm 0.1$  °C), and NIR emissions were recorded on an Edinburgh Analytical Instruments FLS920 lifetime and steady-state spectrometer with a liquid-N<sub>2</sub>-cooled Ge detector with excitation wavelength of 420 and 425 nm. According to the ratio of the slope  $G_{\lambda_{ex}=420\text{ nm}}/G_{\lambda_{ex}=425\text{ nm}}$  (see Figure S1 in the Supporting Information), the quantum yield of YbTPP(Tp) can be reasonably adjusted to 0.043 ( $\lambda_{ex} = 420$  nm), which was used as a reference value for determination of quantum yields of Yb-1 a–5 b. For the quantum-yield determination of Yb-1 a and Yb-1 b, solutions of Yb-1 a, Yb-1 b, and YbTPP(Tp) with three different concentrations were prepared in anhydrous CH<sub>2</sub>Cl<sub>2</sub>. The absorbance of all the solutions at 420 nm were recorded on an Agilent 8453 UV/Vis spectrometer equipped with an Agilent 89090A thermostat ( $\pm 0.1$  °C), and NIR emissions were recorded on an Edinburgh Analytical Instruments FLS920 lifetime and steady-state spectrometer with a liquid-N<sub>2</sub>-cooled Ge detector at an excitation wavelength at 420 nm under an identical condition. According to the ratio of the slope  $G_{Yb-1a}/G_r$  and  $G_{Yb-1b}/G_r$  (see Figure S2 in the Supporting Information), the relative quantum yields of Yb-1 a and Yb-1 b could be obtained according to the above equation. Other Yb porpholactones (Yb-2 a–5 a) and Yb porphyrins (Yb-2 b–5 b) were handled in the same way. The relative uncertainty of the determination can be calculated as

$u = \sqrt{\Delta_r^2 + \Delta_s^2}$ , where  $\Delta_r$  is the relative uncertainty of  $G_r$  and  $\Delta_s$  the relative uncertainty of  $G_s$ . For example, the relative uncertainty for the quantum-yield determination of Yb-1 a can be calculated as  $\sqrt{0.08^2 + 0.05^2} = 9\%$ . The relative uncertainties of other Yb complexes were obtained by the same method and are listed in Table S1 of the Supporting Information. The absorbances of all samples and references were less than 0.1 and were corrected for the background subtracting the average value over the range of 800–820 nm. The integrated emission intensity from 900 to 1100 nm was corrected by subtracting the blank value (integrated emission intensity of pure CH<sub>2</sub>Cl<sub>2</sub> under identical conditions).

**Water titration experiment:** An 80 mM stock solution of 3 in DMSO was prepared, and then a series of solutions with different concentrations of H<sub>2</sub>O (0, 0.278, 0.566, 0.833, 1.39, 1.94, 2.78, 5.56, 8.33, 13.9, 19.4, 27.8 mM) was prepared in a 2 mL volumetric flask. Then, 10 μL of the stock solution of 3 was added to the volumetric flask, and the final concentration of 3 was 4 μM. NIR emissions were recorded on an Edinburgh Analytical Instruments FLS920 lifetime and steady-state spectrometer with a liquid-N<sub>2</sub>-cooled Ge detector at an excitation wavelength of 425 nm under identical conditions at 25 °C.

**Glucose oxidase (GOx) titration experiment:** A series of solutions with different concentrations of GOx (0, 0.0781, 0.156, 0.234, 0.312, 0.469, 0.625, 0.781, 0.938, 1.25, 1.56, 1.87 μM) was prepared by using stock solutions of 3 (80 mM in DMSO) and GOx (1 mg mL<sup>-1</sup> in 50 mM of pH 7.4 Tris-HCl buffer), and the concentration of 3 was 4 μM in each solution. NIR emissions were recorded on an Edinburgh Analytical Instruments FLS920 lifetime and steady-state spectrometer with a liquid-N<sub>2</sub>-cooled Ge detector at an excitation wavelength of 425 nm under identical conditions at 25 °C. The emission intensity monitored at 975 nm was corrected by subtracting the blank value (emission intensity at 975 nm with only pure Tris-HCl buffer under an identical condition).

**Glucose titration experiment:** A stock solution of glucose (400 mM) and 2 mL of a solution containing 3 (4 μM) and glucose oxidase (1.25 μM) in Tris-HCl buffer (50 mM, pH 7.4) were prepared. Then the amount of glucose added to the 2 mL solution was cumulatively increased (0, 1, 2, 3, 7, 10 mM). The volume of total extra solvent was less than 50 μL to keep the total volume nearly unchanged. Sufficient mixing was performed after each addition of glucose. NIR emissions were recorded on an Edinburgh Analytical Instruments FLS920 lifetime and steady-state spectrometer with a liquid-N<sub>2</sub>-cooled Ge detector with excitation wavelength at 425 nm under an identical condition at 25 °C. The emission intensity monitored at 975 nm was corrected by subtracting the blank value (emission intensity at 975 nm of pure Tris-HCl buffer under identical conditions).

## Acknowledgements

Support from NSFC (grant no. 20971007, 21271013 to J.-L.Z.) is gratefully acknowledged.

**Keywords:** biosensors · lanthanides · luminescence · porphyrinoids · ytterbium

- [1] a) M. Pawlicki and L. Latos-Grazynski, in *Handbook of Porphyrin Science* Vol. 2 (Eds: K. M. Kadish, K. M. Smith and R. Guilard), World Scientific, Singapore, 2000, pp. 103–192; b) L. Latos-Grazynski, in *The Porphyrin Handbook*, Vol. 2 (Eds: K. M. Kadish, K. M. Smith and R. Guilard), Academic Press, San Diego, 2000, pp. 361–416; c) M. Toganoh and H. Furuta, in *Handbook of Porphyrin Science* Vol. 2 (Eds: K. M. Kadish, K. M. Smith and

- R. Guillard), World Scientific, Singapore, **2010**, pp. 295–367; d) T. D. Lash, in *Handbook of Porphyrin Science* Vol. 16 (Eds: K. M. Kadish, K. M. Smith and R. Guillard), World Scientific, Singapore, **2010**, pp. 1–330; e) M. Toganoh, H. Furuta, *Chem. Commun.* **2012**, *48*, 937–954.
- [2] a) C. H. Hung, C. K. Ou, G. H. Lee, S. M. Peng, *Inorg. Chem.* **2001**, *40*, 6845–6847; b) H. Furuta, T. Ishizuka, A. Osuka, *J. Am. Chem. Soc.* **2002**, *124*, 5622–5623; c) P. J. Chmielewski, L. Latos-Grazynski, *Coord. Chem. Rev.* **2005**, *249*, 2510–2533; d) H. Maeda, Y. Ishikawa, T. Matsuda, A. Osuka, H. Furuta, *J. Am. Chem. Soc.* **2003**, *125*, 11822–11823; e) I. Gupta, M. Ravikanth, *Coord. Chem. Rev.* **2006**, *250*, 468–518; f) C. Brückner, D. C. G. Gotz, S. P. Fox, C. Ryppa, J. R. McCarthy, T. Bruhn, J. Akhigbe, S. Banerjee, P. Daddario, H. W. Daniell, M. Zeller, R. W. Boyle, G. Bringmann, *J. Am. Chem. Soc.* **2011**, *133*, 8740–8752.
- [3] a) C. P. Wong, R. Venteich, W. D. Horrocks, *J. Am. Chem. Soc.* **1974**, *96*, 7149–7150; b) W. K. Wong, L. L. Zhang, W. T. Wong, F. Xue, T. C. W. Mak, *J. Chem. Soc. Dalton Trans.* **1999**, 615–622; c) T. J. Foley, B. S. Harrison, A. S. Knefely, K. A. Abboud, J. R. Reynolds, K. S. Schanze, J. M. Boncella, *Inorg. Chem.* **2003**, *42*, 5023–5032; d) H. S. He, P. S. May, D. Galipeau, *Dalton Trans.* **2009**, 4766–4771; e) F. Eckes, V. Bulach, A. Guenet, C. A. Strassert, L. De Cola, M. W. Hosseini, *Chem. Commun.* **2010**, *46*, 619–621; f) V. Bulach, F. Sguerra, M. W. Hosseini, *Coord. Chem. Rev.* **2012**, *256*, 1468–1478.
- [4] a) X. J. Zhu, W. K. Wong, W. K. Lo, W. Y. Wong, *Chem. Commun.* **2005**, 1022–1024; b) X. J. Zhu, F. L. Jiang, C. T. Poon, W. K. Wong, W. Y. Wong, *Eur. J. Inorg. Chem.* **2008**, 3151–3162.
- [5] a) M. J. Crossley, L. G. King, *J. Chem. Soc. Chem. Commun.* **1984**, 920–922; b) M. Gouterman, R. J. Hall, G. E. Khalil, P. C. Martin, E. G. Shankland, R. L. Cerny, *J. Am. Chem. Soc.* **1989**, *111*, 3702–3707; c) J. R. McCarthy, H. A. Jenkins, C. Brückner, *Org. Lett.* **2003**, *5*, 19–22; d) C. Brückner, J. Ogikubo, J. R. McCarthy, J. Akhigbe, M. A. Hyland, P. Daddario, J. L. Worlinsky, M. Zeller, J. T. Engle, C. J. Ziegler, M. J. Ranaghan, M. N. Sandberg, R. R. Birge, *J. Org. Chem.* **2012**, *77*, 6480–6494; e) H. B. Lv, B. Y. Yang, J. Jing, Y. Yu, J. Zhang, J. L. Zhang, *Dalton Trans.* **2012**, *41*, 3116–3118; f) Y. Yu, H. Lv, X. Ke, B. Yang, J.-L. Zhang, *Adv. Synth. Catal.* **2012**, *354*, 3509–3516.
- [6] a) B. Zelelow, G. E. Khalil, G. Phelan, B. Carlson, M. Gouterman, J. B. Callis, L. R. Dalton, *Sensor Actuat. B: Chem.* **2003**, *96*, 304–314; b) G. E. Khalil, C. Costin, J. Crafton, G. Jones, S. Grenoble, M. Gouterman, J. B. Callis, L. R. Dalton, *Sensor Actuat. B: Chem.* **2004**, *97*, 13–21; c) M. Gouterman, J. Callis, L. Dalton, G. Khalil, Y. Mebarki, K. R. Cooper, M. Grenier, *Meas. Sci. Technol.* **2004**, *15*, 1986–1994; d) W. Waskitoaji, T. Hyakutake, J. Kato, M. Watanabe, H. Nishide, *Chem. Lett.* **2009**, *38*, 1164–1165; e) W. Waskitoaji, T. Hyakutake, M. Watanabe, H. Nishide, *React. Funct. Polym.* **2010**, *70*, 669–673.
- [7] G. E. Khalil, P. Daddario, K. S. F. Lau, S. Imtiaz, M. King, M. Gouterman, A. Sidelev, N. Puran, M. Ghandehari, C. Brückner, *Analyst* **2010**, *135*, 2125–2131.
- [8] Y. Yu, B. Czepukojc, C. Jacob, Y. Jiang, M. Zeller, C. Brückner, J.-L. Zhang, *Org. Biomol. Chem.* **2013**, *11*, 4613–4621.
- [9] G. Khalil, M. Gouterman, S. Ching, C. Costin, L. Coyle, S. Gouin, E. Green, M. Sadilek, R. Wan, J. Yearyea, B. Zelelow, *J. Porphyrins Phthalocyanines* **2002**, *6*, 135–145.
- [10] a) R. Weissleder, V. Ntziachristos, *Nat. Med.* **2003**, *9*, 123–128; b) J. C. G. Bünzli, *Chem. Rev.* **2010**, *110*, 2729–2755; c) S. V. Eliseeva, J. C. G. Bünzli, *Chem. Soc. Rev.* **2010**, *39*, 189–227.
- [11] X. J. Zhu, P. Wang, H. W. C. Leung, W. K. Wong, W. Y. Wong, D. W. J. Kwong, *Chem. Eur. J.* **2011**, *17*, 7041–7052.
- [12] T. Zhang, X. J. Zhu, C. C. W. Cheng, W. M. Kwok, H. L. Tam, J. H. Hao, D. W. J. Kwong, W. K. Wong, K. L. Wong, *J. Am. Chem. Soc.* **2011**, *133*, 20120–20122.
- [13] W. L. Kwong, R. W. Y. Sun, C. N. Lok, F. M. Siu, S. Y. Wong, K. H. Low, C. M. Che, *Chem. Sci.* **2013**, *4*, 747–754.
- [14] a) G. A. Crosby, J. N. Demás, *J. Phys. Chem.* **1971**, *75*, 991–1024; b) A. T. R. Williams, S. A. Winfield, J. N. Miller, *Analyst* **1983**, *108*, 1067–1071; c) J. Zhang, P. D. Badger, S. J. Geib, S. Petoud, *Angew. Chem.* **2005**, *117*, 2564–2568; *Angew. Chem. Int. Ed.* **2005**, *44*, 2508–2512; d) J. Zhang, S. Petoud, *Chem. Eur. J.* **2008**, *14*, 1264–1272; e) E. G. Moore, J. Grilj, E. Vauthey, P. Ceroni, *Dalton Trans.* **2013**, *42*, 2075–2083; f) *A Guide to Recording Fluorescence Quantum Yields*, HORIBA Jobin Yvon Inc. <http://www.jobinyvon.com/usadivisions/fluorescence/applications/quantumyieldstrad.pdf>.
- [15] G. A. Crosby, R. M. Alire, R. E. Whan, *J. Chem. Phys.* **1961**, *34*, 743–748.
- [16] B. Wardle, *Principles and Applications of Photochemistry*, John Wiley & Sons, Ltd, West Sussex, UK, **2009**, pp. 77–79.
- [17] A. Beeby, I. M. Clarkson, R. S. Dickens, S. Faulkner, D. Parker, L. Royle, A. S. de Sousa, J. A. G. Williams, M. Woods, *J. Chem. Soc. Perkin Trans. 2* **1999**, 493–503.
- [18] Lakowicz JR, *Principles of fluorescence spectroscopy*, Springer, Singapore, **2006**, pp. 277–330.
- [19] a) M. J. Rogers, K. G. Brandt, *Biochemistry* **1971**, *10*, 4624–4630; b) R. Wilson, A. P. F. Turner, *Biosens. Bioelectron.* **1992**, *7*, 165–185.
- [20] H. S. He, J. P. Guo, Z. X. Zhao, W. K. Wong, W. Y. Wong, W. K. Lo, K. F. Li, L. Luo, K. W. Cheah, *Eur. J. Inorg. Chem.* **2004**, 837–845.
- [21] X. Chen, L. Hui, D. A. Foster, C. M. Drain, *Biochemistry* **2004**, *43*, 10918–10929.

Received: October 10, 2013

Revised: December 20, 2013

Published online on March 3, 2014